Proceedings of the ASME Turbo Expo 2013
TEC2013
June 03-07, 2013, San Antonio, Tx, USA

GT2013-95694

A HYBRID IMMERSED BOUNDARY CFD APPROACH TO OIL & GAS APPLICATIONS

Marco Mulas*
KARALIT s.r.l.
Pula, 09010
Italy
Email: marco.mulas@karalit.com

Marco Talice
KARALIT s.r.l.
Pula, 09010
Italy
marco.talice@karalit.com

Annabella N. Grozescu
KARALIT s.r.l.
Pula, 09010
Italy
annabella.grozescu@karalit.com

ABSTRACT

In the past decade a large degree of advancement has been made in CFD labs worldwide, towards the development of Immersed Boundary (IB) CFD methods. The IB method belongs to a new class of numerical methods sometime called mesh-less methods, as no standard meshes that conform to the geometry (or body) need to be generated. The discrete points where the calculation is performed can be freely distributed in the computational domain without great concern for the position of the geometry. The geometry is immersed into a Cartesian grid and the methodology accounts for the effects of the presence of the body in the flow field. The IB method therefore frees up the user from the time consuming and often complicated need for meshing. Plenty of proofs of accuracy and validations are presented yearly at the most prestigious CFD conferences and are available on the internet. Oil and Gas CFD applications are concerned with a variety of internal flow problems. Most of those problems present geometrical complexities, valves for instance, that make a standard body-fitted generation of good quality meshes almost an impossible task. And bad inputs, such as low quality meshes, always determine bad outputs, low quality results. In this paper the KARALIT CFD code based on a class of IB methodology akin to ghost cell methods, is applied to a class of applications encountered often in oil and gas plants, namely a pipeline connecting an arbitrary number of valves, or other devices. While complex valves and devices do make the standard body-fitted approach extremely tedious and difficult, on the other side pipelines are naturally and easily modeled using standard body-fitted cylindrical meshes. The hybrid CFD approach presented will show an automatic implementation of mixed type domain: pipes cylindrical body-fitted meshes are automatically generated by the method and automatically connected to the devices which are treated with the IB method. Examples of lines with arbitrary number of devices will be shown. Result and key performance parameters are provided from the IB CFD calculations and key conclusions about the line characteristic are drawn.

NOMENCLATURE

C_p	Specific heat
E	Total energy
Pr	Prandtl number
T	Temperature
d	Distance from the closest surface
e	Internal specific energy
k	Turbulent kinetic energy
p	Pressure
t	Time
u_i	Velocity components
γ	Ratio of specific heats
μ	Dynamic viscosity
ν	Kinematic viscosity
Ω_{ij}	Rotation tensor
ρ	Density
τ_{ji}	Viscous stress tensor
$\tilde{()}$	Density weighted time-average of quantity
$\bar{()}$	Time average of quantity
$()^{\text{“}}$	Fluctuating quantity
$()_t$	Turbulent quantity

*Address all correspondence to this author.

INTRODUCTION

Valves used in the Oil and Gas industries can have relevant dimensions, with typical diameters of some 2 $[m]$ or above. Those valves operate at nominal and off-design conditions characterized by mass flow rate values of tens of $[kg/s]$ of gas, which make unpractical and far too expansive running any experimental test. Even though semi-empirical methods are still used in valves' design, the diffusion of Computational Fluid Dynamics (CFD) in recent years and the market's and regulators' requirement of numerical validations, resulted in a wider use of numerical simulations of valves' lines. The very first step of any CFD study is the discretization of the domain into computational cells, over which the set of equations that describes the dynamics of fluids are integrated. This phase of the process is known as grid generation and for complicated geometries like valves', it can be really time consuming. Moreover, this activity usually requires highly skilled operators, who are not typically available in this kind of industry. In the past decade the Immersed Boundary Method has started coming out from the academic environment into which has been confined, and has been used successfully on a number of applications of real industrial interest, ranging from automotive to bio-medical ones. The most apparent advantage of this class of methods over traditional CFD tools is that the above mentioned meshing process is almost entirely skipped, resulting in a great saving in the overall simulation cost.

The present paper deals with the application of a hybrid IB method to a real case of industrial interest. Valves are inserted into a pipe line to ensure that a desired pressure drop is realized along the line. As the insertion of a valve into a line perturbs the flow downstream the valve itself, it is a commonly used guideline to leave a proper distance (usually several diameters) in between two consecutive valves. Sometimes, because of a particular plant's layout, it is not possible to satisfy this best practice requirement. It becomes then interesting to understand the implication that such a non standard layout has on the flow field inside the piping and on the system at large.

In the first part of the paper a brief historical review of the several kinds of IB methods is presented, together with a summary of the equations which are to be solved. Then a particular type of IB method, the Ghost Cell Method, is presented, outlining the logical steps in which the method articulates. Finally, results obtained on the above mentioned test case are presented and some conclusions are driven.

NUMERICAL METHOD

The code KARALIT CFD is based upon the Ghost Cells method, which belongs to the more general class of IB methods. The idea behind this class of methods is the decoupling between the actual geometry of the fluid domain and the underlying grid which is used for the integration of the flow dynamics equations. The main advantage of this approach is that simple regular meshes (e.g. Cartesian) can be used, thus retaining all the ease and efficiency of the numerical methods developed in that framework. The effect on the flow field of a stationary or moving boundary is accounted for by the introduction of a distribution of fictitious forcing terms in the governing equations, such that the correct flow boundary conditions on solid boundaries can be assigned. The first example of this methodology can be found in Vieceli [1]. His original idea was to consider the fluid-boundary interface as a free-surface and to impose there pressure boundary conditions so that fluid particles could move only along the tangent to the boundary line. The method was generalized in a successive paper [2] to include the possibility of walls either moving with a prescribed law or moving as a consequence of the forces exerted by the fluid on the surface. The method has achieved a certain degree of popularity during the seventies, when Peskin [3, 4] successfully simulated a two-dimensional stream of blood inside a hearth mitral-valve with a very low Reynolds number. The first three-dimensional heart flows simulations that included also the contractile and elastic nature of the boundary were successively carried out by Peskin himself [5] and by McQueen and Peskin [6, 7]. The first applications of the method to problems with an immersed, solid and undeformable surface are found in Basdevant and Sadourny [8], Briscolini and Santangelo [9], and Goldstein et al. [10]. Up to that point the method was successfully applied to simple geometries and to laminar flows.

The first examples of application of the method to complex problems of industrial and biologic relevance can be found in Fadlun et al. [11] where the flow inside an internal combustion piston/cylinder assembly is investigated; in Balaras [12] the fully developed turbulent flow in a plane channel with a wavy wall is considered; Majumdar et al. [13] study the laminar flow around a semi-circular cylinder at Reynolds number of 150, as well as the laminar flow past a two-dimensional bump and the fully developed turbulent flow in a plane two-dimensional channel; Tseng and Ferziger [14] apply the methodology to the study of geophysical flows over a three-dimensional bump, whereas Iaccarino [15] investigates several kind of flows, namely, the flow in a wavy channel, the flow over a turbine blade, the flow in a rib-roughened serpentine, the flow around a pick-up truck, and finally, the flow around a Ferrari F50 overcoming a Porsche 911; Dadone and Grossman [16, 17] focus their attention on several flows of aerospace interest, such as the transonic flow around a NACA 0012 airfoil, the flow over a bi-NACA configuration and the transonic flow over the ONERA M6 wing. Poncet [18] simulates three-dimensional flows around an aircraft model and a bridge. Borazjania et al. [19] carry out the simulation of the fluid structure interaction with complex 3D rigid bodies. In particular, the vortex induced vibration of elastically mounted cylinders and the flow through a bi-leaflet mechanical heart valve at physiologic conditions are simulated.

The method used in the present work is known as *Ghost*

Cells method. In order to inform the flow field of the presence of an immersed solid body, the system of the fluid dynamics equations must be completed with an extra term, usually named a forcing term. It is demonstrated [16] that this extra forcing term reduces to the imposition of proper boundary conditions. This is particularly appealing because no modification to the equations has to be introduced and the same numerical methods that are traditionally used to integrate the Navier-Stokes equations still hold valid.

Governing Equations

The equations governing the motion of a turbulent flow of a compressible and viscous fluid are the so called Favre-averaged Navier-Stokes equations. They represent conservation laws of mass, momentum and energy. If neglecting body forces, these equations can be written in Cartesian coordinates as:

$$\frac{\partial \bar{\rho}}{\partial t} + \frac{\partial}{\partial x_j}\left(\bar{\rho}\widetilde{u_j}\right) = 0 \tag{1}$$

$$\frac{\partial(\bar{\rho}\widetilde{u_i})}{\partial t} + \frac{\partial}{\partial x_j}\left[\bar{\rho}\widetilde{u_j}\widetilde{u_i} + \bar{p}\delta_{ij} - \widetilde{\tau_{ji}^{tot}}\right] = 0 \tag{2}$$

$$\frac{\partial(\bar{\rho}\widetilde{E})}{\partial t} + \frac{\partial}{\partial x_j}\left[\bar{\rho}\widetilde{u_j}\widetilde{E} + \widetilde{u_j}\bar{p} + \widetilde{q_j^{tot}} - \widetilde{u_i}\widetilde{\tau_{ij}^{tot}}\right] = 0 \tag{3}$$

where $\widetilde{E}$ is the total energy per unit mass:

$$\widetilde{E} = \widetilde{e} + \frac{\widetilde{u_k}\widetilde{u_k}}{2} + k \tag{4}$$

where k is the turbulent kinetic energy, which is defined as:

$$k \equiv \frac{\widetilde{u_k''u_k''}}{2} \tag{5}$$

and

$$\widetilde{\tau_{ij}} \equiv \mu\left(\frac{\partial \widetilde{u_i}}{\partial x_j} + \frac{\partial \widetilde{u_j}}{\partial x_i} - \frac{2}{3}\frac{\partial \widetilde{u_k}}{\partial x_k}\delta_{ij}\right) \tag{6}$$

$$\widetilde{q_j} \equiv -C_p\frac{\mu}{Pr}\frac{\partial \widetilde{T}}{\partial x_j} \tag{7}$$

being $\widetilde{q_j}$ the heat flux components.

The above formulation is strictly valid for compressible flows. Its extension to the incompressible regime is achieved via preconditioning [20]. Numerical fluxes and source terms are multiplied by a preconditioning matrix $\mathbf{P}$. The Navier-Stokes system can be written in compact vector form as:

$$\frac{\partial Q}{\partial t} + \mathbf{P}\left(\frac{\partial F_x}{\partial x} + \frac{\partial F_y}{\partial y} + \frac{\partial F_z}{\partial z}\right) + \mathbf{P}\left(\frac{\partial G_x}{\partial x} + \frac{\partial G_y}{\partial y} + \frac{\partial G_z}{\partial z}\right) = \mathbf{P}S \tag{8}$$

where $\overrightarrow{F}$ and $\overrightarrow{G}$ are the inviscid and viscous flux vectors and S is the source term array. The preconditioning matrix is given by $\mathbf{P} = \mathbf{M}\mathbf{M}_m^{-1}$. $\mathbf{M}$ represents the Jacobian matrix of the vector of conservative variables $Q\left(\rho, \rho\overrightarrow{V}, \rho E\right)$ with respect to the vector of the viscous-primitive variables $Q_v\left(p, \overrightarrow{V}, T\right)$. $\mathbf{M}_m$ represents a modified version of $\mathbf{M}$. No modification brings back the original non-preconditioned system ($\mathbf{P} = \mathbf{I}$).

The turbulent eddy viscosity μ_t is obtained from a turbulence model. The one equation Spalart and Allmaras model [21] has been used throughout all simulations. The model formulation in compressible form writes as:

$$\frac{\partial \widetilde{\nu}}{\partial t} + \frac{\partial}{\partial x_j}\left(\widetilde{\nu}u_j\right) = C_{b1}\left[1 - f_{t2}\right]\widetilde{S}\widetilde{\nu} + \frac{1}{\sigma}\left\{\bigtriangledown\cdot\left[\left(\nu + \widetilde{\nu}\right)\bigtriangledown\widetilde{\nu}\right] + C_{b2}\left|\bigtriangledown\nu\right|^2\right\} - \left[C_{w1}f_w - \frac{C_{b1}}{\kappa^2}f_{t2}\right]\left(\frac{\widetilde{\nu}}{d}\right)^2 + f_{t1}\triangle U^2 \tag{9}$$

$$\widetilde{S} \equiv S + \frac{\widetilde{\nu}}{\kappa^2 d^2}f_{v2} \qquad f_{v2} = 1 - \frac{\chi}{1 + \chi f_{v1}} \tag{10}$$

where:

$$S \equiv \sqrt{2\Omega_{ij}\Omega_{ij}} \qquad \Omega_{ij} \equiv \frac{1}{2}\left(\frac{\partial u_i}{\partial x_j} - \frac{\partial u_j}{\partial x_j}\right) \tag{11}$$

Ω_{ij} being the strain rate tensor.

$$f_w = g\left[\frac{1 + C_{w3}^6}{g^6 + C_{w3}^6}\right]^{\frac{1}{6}}, g = r + C_{w2}\left(r^6 - r\right), r \equiv \frac{\widetilde{\nu}}{\widetilde{S}\kappa^2 d^2} \tag{12}$$

$$f_{t1} = C_{t1} g \; exp\left(-C_{t2}\frac{\omega_t^2}{\triangle U^2}\left[d^2 + g^2 d^2\right]\right) \tag{13}$$

$$f_{t2} = C_{t3} exp\left(-C_{t4}\chi^2\right) \tag{14}$$

For the wall boundary condition to be satisfied, μ_t has to be equal to 0 at solid walls. The eddy-viscosity is:

$$\nu_t = \widetilde{\nu} f_{v1}, \qquad \mu_t = \rho \widetilde{\nu} f_{v1} \tag{15}$$

$$f_{v1} = \frac{\chi^3}{\chi^3 + C_{v1}^3}, \qquad \chi = \frac{\widetilde{\nu}}{\nu} = \kappa y^+ \tag{16}$$

In the Spalart-Allmaras model, the correct near wall behavior of ν_t is ensured by the introduction of f_{v1}, which is a function of the non dimensional wall distance y^+. Function f_{v1} is such that for $y^+ = 0$, $f_{v1} = 0$ and for high values of y^+, $f_{v1} = 1$, which satisfies $\nu_t = \widetilde{\nu}$ outside the boundary layer.

The model's constants are [21]:

$$\sigma = \frac{2}{3}, \quad C_{b1} = 0.1355, \quad C_{b2} = 0.622, \quad \kappa = 0.41$$
$$C_{w1} = \frac{C_{b1}}{\kappa^2} + \frac{(1 + C_{b2})}{\sigma}, \quad C_{w2} = 0.3, \quad C_{w3} = 2.0, \quad C_{v1} = 7.1$$
$$C_{t1} = 1.0, \quad C_{t2} = 2.0, \quad C_{t3} = 1.2, \quad C_{t4} = 0.5 \tag{17}$$

The Ghost Cells Method

As it has been stated above the Ghost Cell method reduces into imposing proper boundary conditions to take into account the existence of a solid body inside the Cartesian grid that represents the computational domain. Following the formulation proposed by Dadone and Grossman [16, 22] and with reference to Fig. 1, this can be accomplished by the following logical steps:

1. The body's geometry is provided in some CAD output form. In the case of KARALIT CFD the expected input file is a triangulated surface in stereo-lithography format (STL).
2. The body, which is shown in gray color in Fig. 1, is immersed into a Cartesian grid, which is completely independent of the body itself (non conformal to the body surface definition).
3. The grid's cells are labeled based on the position of their centers with respect to the body. With reference to Fig. 1, cells are classified as: fully fluid cell (FC) when the cell falls entirely inside the fluid region; fully solid cell (SC) when the cell falls entirely inside the body; boundary cell (BC) when the cell is cut by the body but its center is on the fluid side; ghost cell (GC) when the cell is cut by the body but its center is on the solid side. For a second order method it is usually necessary to identify two rows of ghost cells. The fully solid cells do not enter the computation and are neglected by the method.
4. The position of each ghost cell is reflected into the fluid region by mirroring the cell along the normal to the body surface passing through the cell center.
5. All flow variables are reconstructed at each of those mirror points (MP) via an interpolation procedure which involves a given number of fluid cells surrounding the mirror point itself.
6. The computed variables at mirror points are reflected back to the original ghost cells and are used to enforce the desired boundary conditions (e.g. no-slip condition for velocity at walls).

Once points 1 to 6 above have been completed, the same numerical schemes which are used to integrate the Navier-Stokes equation on body-conformal meshes can be applied. A second order Total Variation Diminishing (TVD) Roe's flux splitting method [20] has been used to integrate the system in space and an implicit method has been applied to advance solution in time.

In order to reduce the overall number of computational cells, the software automatically generate a cylindrical body-conformal mesh inside the pipe elements connecting the valves. The use of a Cartesian mesh on those cylindrical line elements would in fact result in an increased number of cells and therefore computational time, without giving any advantage due to their simple geometrical shape. In this sense the approach is to be considered hybrid. At the interface between the Cartesian and cylindrical meshes, an interpolation procedure is applied. The two grids are displayed in Fig. 2.

TEST CASE

The goal of the present study is to assess the performance of three different assemblies of a combination of three valves, whose actual geometrical definition has been provided by a company operating in the sector. The valves, whose common diameter is 1.75 $[m]$, are shown in the Fig. 3. Element E1 is the assembly of a Flue Gas valve and a Butterfly valve. Elements E2 and E3 are both Butterfly valves, which differ for their spatial orientation. Discs of all Butterfly valves are orientated at 45° respect to the center-line. Element E3 has been obtained by rotating element E2 by 90° around the center-line so that the rotation axes of the discs are now placed on orthogonal planes. Elements E1, E2 and E3 have been assembled into three different line configurations, which are illustrated in Fig. 4. Configurations differ for the length of the pipe which connects the elements. Two pipes

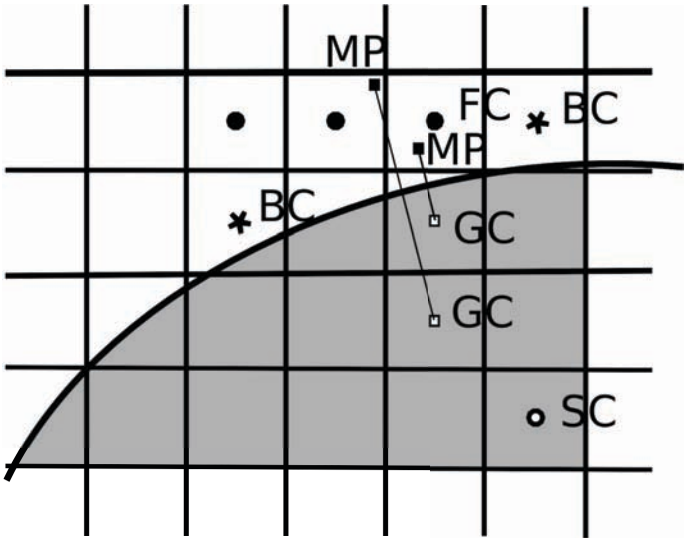

FIGURE 1. CLASSIFICATION OF COMPUTATIONAL CELLS OVER THE CARTESIAN GRID. THE GRAY COLOR REPRESENTS THE SOLID SIDE.

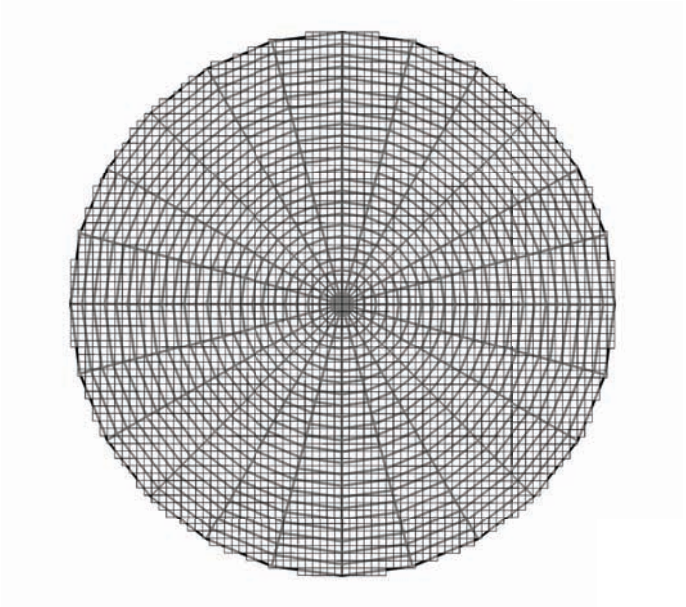

FIGURE 2. THE HYBRID CYLINDRICAL BODY-CONFORMAL/CARTESIAN MESH; INTERPOLATION IS USED TO TRANSFER INFORMATION BETWEEN GRIDS.

have been used for the present study, the first having a length of about 6 valve diameter (long pipe) and the second one of about 1 valve diameter (short pipe). Configuration C1 uses the long pipe to connect elements E1 and E2. Configuration C2 uses the short

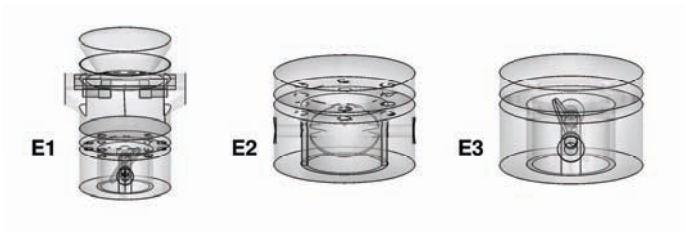

FIGURE 3. THE THREE ELEMENTS (E1, E2, E3) USED THROUGHOUT THE SIMULATIONS.

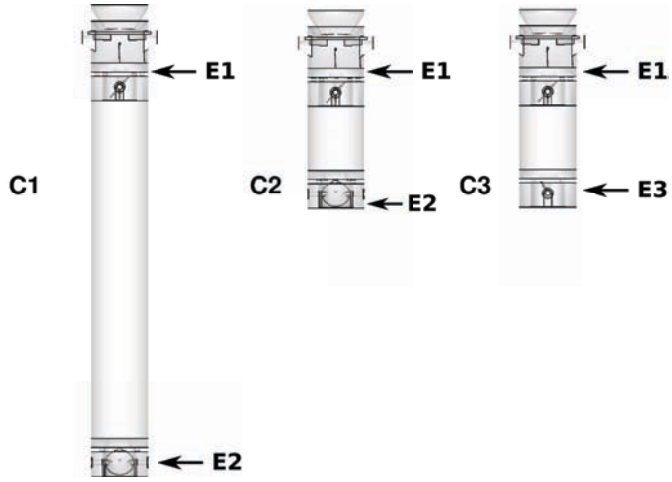

FIGURE 4. THE THREE ASSEMBLY CONFIGURATIONS (C1, C2, C3) USED THROUGHOUT THE SIMULATIONS.

pipe in between elements E1 and E2, whereas configuration C3 uses the short pipe in between elements E1 and E3.

Aim of the simulation is to provide an assessment of the overall line performance (pressure drop) as well as of the influence of the pipe's length over the flow field structure inside the line. The problem is of real industrial relevance as sometimes in actual Oil and Gas plants' layouts it is not possible to fit pipes long enough in between line elements to meet the theoretical conditions for the operation of the line.

Simulation Set-up

The three configurations have been simulated by using the "Valve Line App" which is available in the CFD code KARALIT CFD. As the code is based upon an IB method, no meshing is required. The geometrical description of each line element is imported in STL format and the software takes care of automatically generating the pipes according to the prescriptions given by the user. Valves are immersed into a Cartesian grid, whereas a body conformal grid is created by the software on the pipes. An example of the mesh is given in Fig. 5.

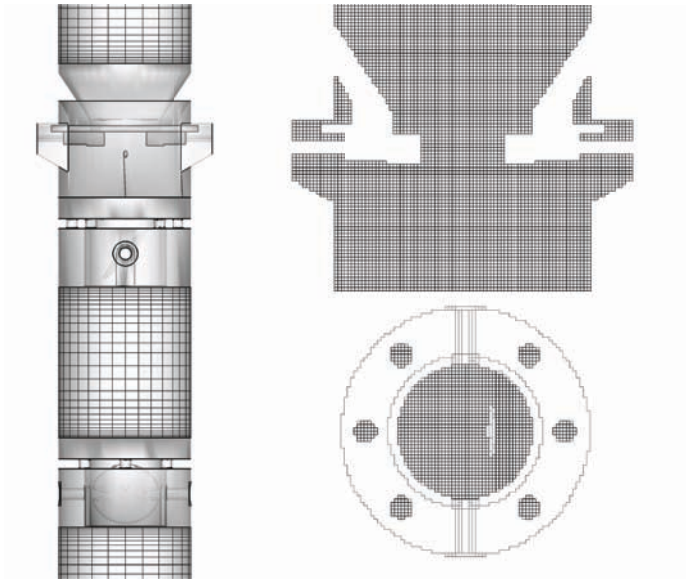

FIGURE 5. VALVE LINE RENDERING AND GRID. A CILINDRICAL BODY CONFORMAL GRID IS CREATED OVER THE PIPES (LEFT); VALVES ARE IMMERSED INTO A CARTESIAN GRID (RIGHT).

Steady state simulations have been carried out for a turbulent compressible flow. An implicit time advancing scheme has been used throughout the simulations. The CFL (Courant–Friedrichs–Lewy) number [23] has been set to be 100 for configuration C1 and 10 for configurations C2 and C3. A second-order accurate symmetric TVD scheme has been used for space discretization. No-slip conditions have been applied to all solid walls. A mass flow rate of 69 024 $[kg\ \ s]$ and a temperature of 983 15 $[K]$ have been imposed at the line inlet, whereas a uniform pressure value of $p = 109725$ $[Pa]$ has been set as outlet condition. The Reynolds number based on the inlet velocity and pipe diameter is approximately 2 8 10^6, therefore the flow is to be considered fully turbulent.

Turbulence has been taken into account by using the Spalart-Allmaras model, with an inlet value of the resolved turbulent eddy viscosity equal to 1 $0E^{04}$ $[m^2\ \ s]$. The evolving fluid is a mixture whose main components are Hydrogen, Ethane and Methane that can be regarded to be an ideal gas with a density equal to 0 84 $[kg\ \ m^3]$.

RESULTS AND DISCUSSION

In order to assess the grid independence of the computed results, simulation of configuration C2 has been carried out on three different grid levels. Table 1 reports a summary of grid sizes and computed values for the pressure drop between inlet and outlet line sections. As the variation of the computed pressure drop value p stays inside a 5 0% difference range while moving from grid 2 to grid 3, the grid 2 has been chosen for all simulations.

TABLE 1. GRID SENSITIVITY ANALYSIS.

Grid	Total number of cells	p $[kPa]$	Variation $[\%]$
1	272000	156	-
2	1550000	130	16.7
3	5000000	129	0.7

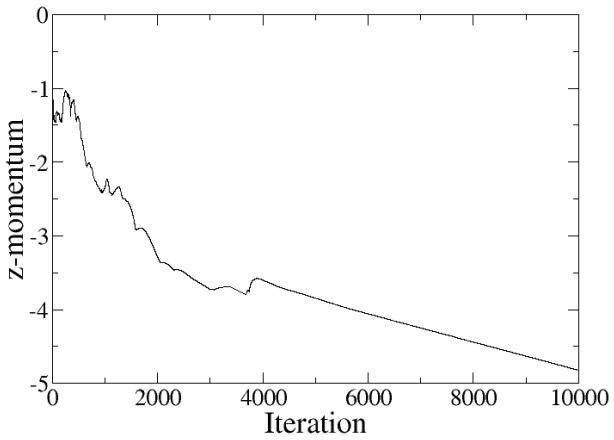

FIGURE 6. CONVERGENCE HISTORY OF NORMALIZED Z-MOMENTUM RESIDUAL.

It has been estimated a posteriori that y^+ at the first grid node is in the range of $[4;370]$ in grid 2 and $[1;290]$ in grid 3.

Figure 6 shows the numerical convergence history of the normalized z-momentum residual (along the pipe line axis). A further assessment of having reached a fully converged solution is given by Figs. 7 and 8 which represent the solution history of the mass flow rate and of the average pressure values inside the pipes. The absence of periodic oscillations in the convergence history indicates that the average flow is steady in nature and that the flow filed configuration is not time dependent.

Table 2 reports the computed values of the pressure drop. The expected value, as calculated using semi-empirical 1-D formulas for both the Butterfly valve ([24]) and Flue Gas valve is of about 125 $[kPa]$. Formulas cannot be reported herein as they are subject to copyright issues enforced by the Process Licensor. Figures 9 and 10 show relative pressure profiles along the assembly center-line for the three configurations. While Tab.

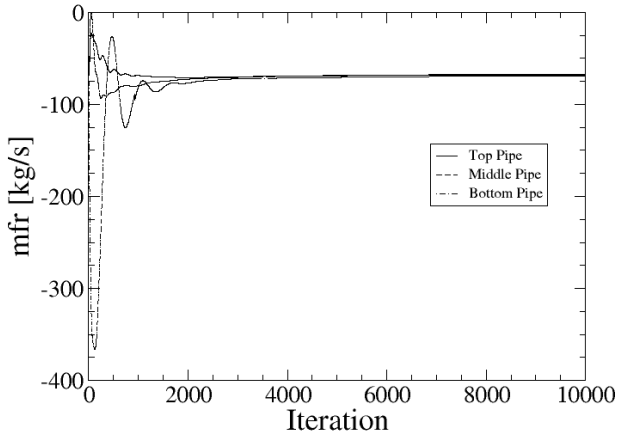

FIGURE 7. CONVERGENCE HISTORY OF THE MASS FLOW RATE INSIDE THE THREE PIPES.

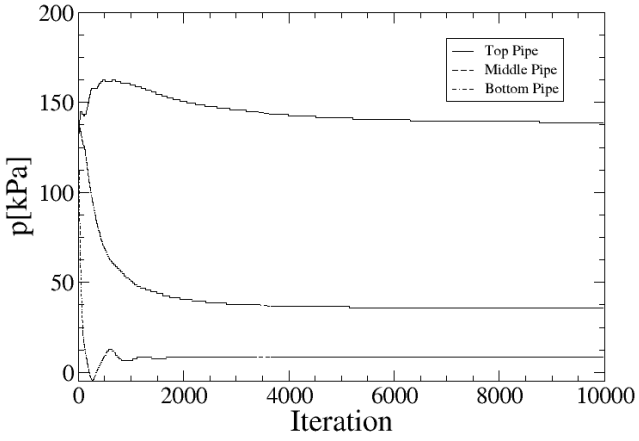

FIGURE 8. CONVERGENCE HISTORY OF AVERAGE RELATIVE PRESSURE INSIDE THE THREE PIPES.

2 shows that the overall pressure drop does not change significantly in all simulated cases, a few comments can be done on the pressure distribution inside the three different assemblies. Comparison of Figs. 9 and 10 shows that there is a substantially equal pressure drop through elements E1 and E2. Some differences can be pointed out for the pressure distribution inside the pipe in between those elements. Particularly, pressure seems to reach a plateau inside the long pipe of configuration C1, whereas it shows a steep slope inside the short pipe of configurations C2

TABLE 2. COMPUTED PRESSURE DROP

Configuration	$p[kPa]$
C1	132
C2	130
C3	130

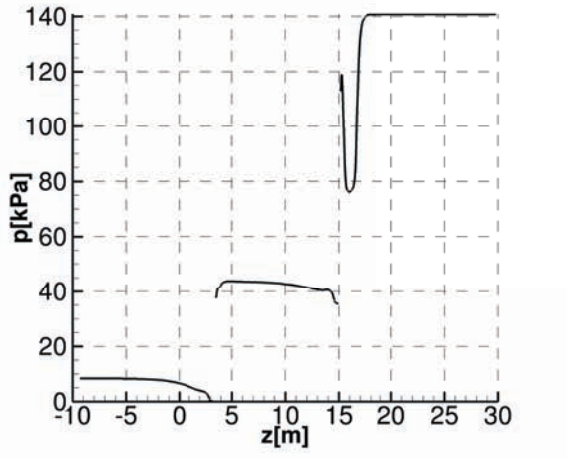

FIGURE 9. RELATIVE PRESSURE ALONG THE VALVE LINE'S AXIS (CONFIGURATION 1).

and C3. This can possibly be an indication of a more chaotic behavior of the fluid inside the shorter pipe compared to what happens inside the longer one. This phenomenon will be further investigated later on while discussing the flow patterns inside the assemblies. Analysis of the same Fig. 10 shows how the use of element E3 instead of element E2 in the short pipe configuration does not produce any significant change into the pressure distribution along the center-line of the assembly.

Figures 11, 12 and 13 show the flow's streamlines on two orthogonal meridian planes and on relevant cross sections along the pipe. The existence of two stationary vortexes can be noticed in Fig. 11. Position of those vortexes does not vary in time and their combined action results into the creation of a fluid nozzle whose throat section forces the fluid to accelerate in the first part of the pipe and then to recover its original pressure level in the diverging part of the fluid nozzle. This positive pressure gradient is shown also in the above mentioned Fig. 9, where it can be seen that along the pipe's axis pressure slightly increases from its value at the downstream element E1 until the end of the pipe. The smooth pressure distribution results from an ordered behavior of

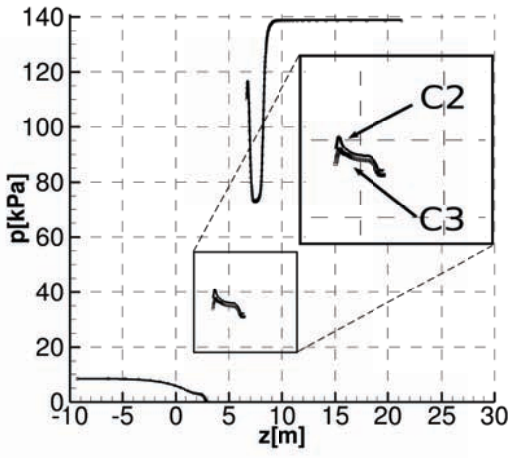

FIGURE 10. RELATIVE PRESSURE ALONG THE VALVE LINE'S AXIS (CONFIGURATIONS 2 AND 3).

the fluid inside the long pipe. Flow patterns on the cross sections shown on the right hand side of Fig. 11, suggest the absence of vorticity on planes orthogonal to the pipe axis. This is a further indication of a well established and ordered flow regime.

Figures 12 and 13 allow to state that the flow inside configurations C2 and C3 behaves substantially in the same way. A stationary system of two vortexes exists on both meridian planes and those vortexes show no symmetry with respect to the pipe axis. Their position and intensity appear to be almost the same for both configurations. Exam of Figs. 12 and 13 shows that a sort of fluid nozzle also exists, but its throat cross section dimension is smaller than that that characterizes configuration C1, namely about 0 73 $[m]$ versus about 0 78 $[m]$. Moreover, this nozzle appears to be slightly angled with respect to the axial direction. A somewhat more noticeable difference can be evidenced on the cross sections **A-A** which have been taken at the same axial position. A system of three vortexes exists on both configurations but the intensity of those in the upper part of section **A-A** appears to be higher in configuration C3 than in configuration C2. The opposite holds true for the smaller vortex in the lower part of the same section.

Figure 14 illustrates the Mach number iso-line distribution on the same meridian plane for each of the three configurations. Even though the Mach number is rather low (0 053) at the inlet, it reaches its maximum values of about 0 78 and 0 80 for configuration C1 and configurations C2 and C3, respectively, in the lower part of the butterfly disc of element E1. Rather high values are also found downstream the circumferential by-pass holes. This wide range of Mach number inside the flow field justifies the adoption of a compressible formulation for solving the fluid dynamics equations.

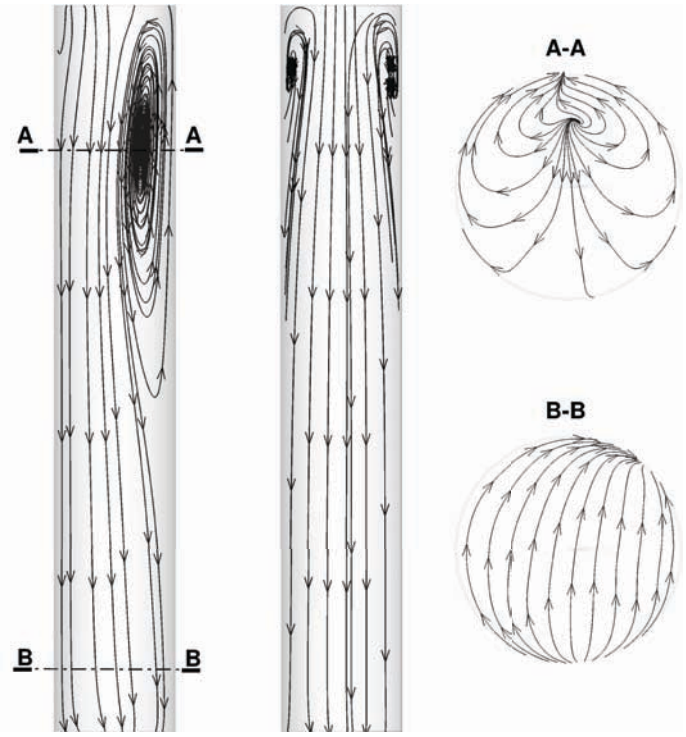

FIGURE 11. STREAMLINES (CONFIGURATION C1: ELEMENTS E1, E2 CONNECTED BY LONG PIPE).

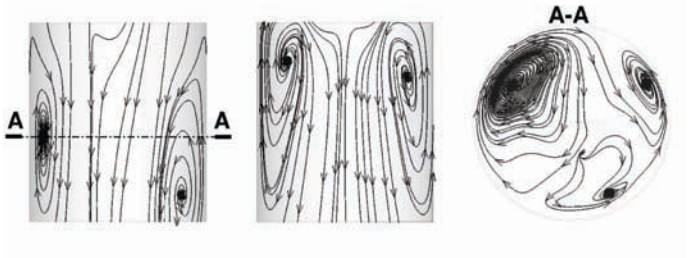

FIGURE 12. STREAMLINES (CONFIGURATION C2: ELEMENTS E1, E2 CONNECTED BY SHORT PIPE).

Figure 15 shows the temperature iso-line distribution on the same pipe's cross sections **A-A** already used in Figs. 11, 12 and 13. The considered temperature range is the same (960 970 $[K]$) for configurations C1 and C2, but the colder flow core center results closer to the wall in configuration C1 than in configuration C2. This is due to the absence of vorticity on the left hand side of the meridian plane, as visible in Fig. 11. Although the temperature range is the same for the two cases, temperature distribution results globally more uniform in configuration C1, with a less steep temperature gradient. This is evi-

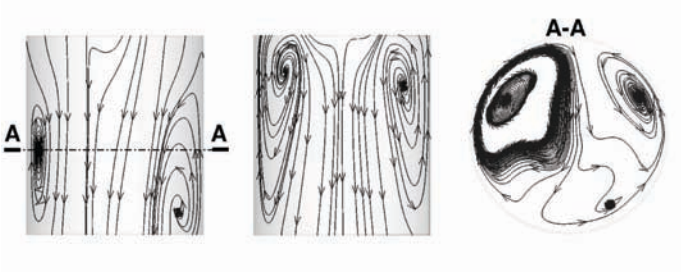

FIGURE 13. STREAMLINES (CONFIGURATION C3: ELEMENTS E1, E3 CONNECTED BY SHORT PIPE)

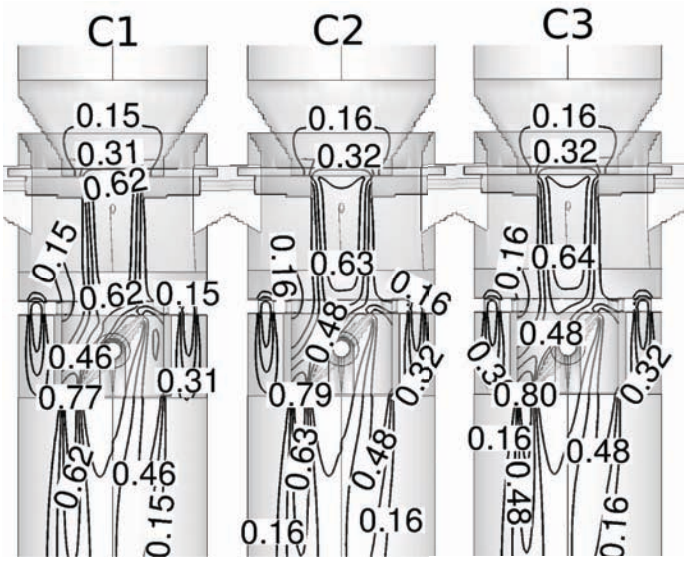

FIGURE 14. MACH NUMBER CONTOUR PLOT (CONFIGURATIONS C1, C2 AND C3)

denced by a more spread iso-lines distribution. Comparison of configurations C2 and C3 shows that the colder fluid core position is almost the same, but the maximum temperature value in configuration C3 results to be reduced by some 5 $[K]$. This can be the effect of a more intense mixing induced by the stronger vorticity already discussed in Fig. 13.

CONCLUSIONS

A hybrid IB method has been applied to the simulation of a realistic Oil and Gas case. The study has allowed for a better understanding of what happens inside the system when the length of the pipe connecting two consecutive valves is shortened with respect to what the standard best practice would suggest. The methodology makes possible to easily change the relative position of the valves' line elements with no particular effort and

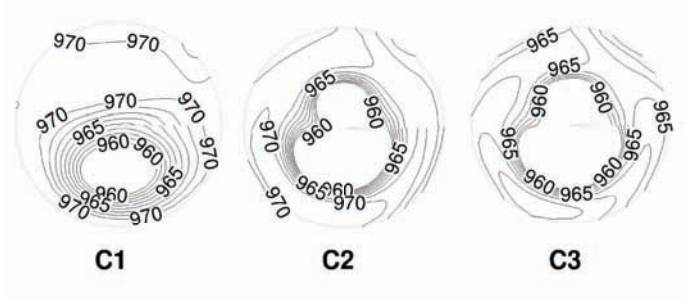

FIGURE 15. TEMPERATURE ISO-LINES ON THE PIPE'S CROSS SECTION AT MAXIMUM VORTICITY.

without any need of meshing. It has been seen that the recirculating flow inside the pipe modifies as the pipe length is reduced, increasing the overall level of disorder in the flow and resulting in a less uniform distribution of velocity and temperature. Moreover, the angular position of the third line element has been changed in order to assess the eventual influence of a different spatial position of the Butterfly valve's disc on the flow behavior. It has been found that the only visible influence is registered on temperature's distribution and peak value. In all cases, the overall pressure drop remains virtually unchanged and similar to what was expected from the use of semi-empirical one-dimensional formulas.

PAPER NUMBER

GT2013-95694

ACKNOWLEDGMENT

We would like to thank Remosa SpA (an IMI Company) for the support provided throughout the present work.

REFERENCES

[1] Vieceli, J., 1969. "A Method for Including Arbitrary External Boundaries in the MAC Incompressible Fluid Computing Technique". *Journal of Computational Physics,* ***4***(4), December, pp. 543–551.

[2] Vieceli, J., 1971. "A Computing Method for Incompressible Flows Bounded by Moving Walls". *Journal of Computational Physics,* ***8***(1), August, pp. 119–143.

[3] Peskin, C., 1972. "Flow Patterns Around Heart Valves: A Digital Computer Method for Solving the Equations of Motion". PhD Thesis, Albert Einstein College of Medicine, Yeshiva University. University Microfilms no. 72-30, 378.

[4] Peskin, C., 1977. "Numerical Analysis of Blood Flow in the Heart". *Journal of Computational Physics,* ***25***(3), November, pp. 220–252.

[5] Peskin, C., 1982. "The Fluid Dynamics of Heart Valves: Experimental, Theoretical and Computational Methods". *Annual Review of Fluid Mechanics,* ***14***, January, pp. 235–259.

[6] Peskin, C., and McQueen, D., 1989. "A Three-Dimensional Computational Method for Blood Flow in the Heart: (I) Immersed Elastic Fibers in a Viscous Incompressible Fluid". *Journal of Computational Physics,* ***81***(2), April, pp. 372–405.

[7] McQueen, D., and Peskin, C., 1989. "A Three-Dimensional Computational Method for Blood Flow in the Heart: (II) Contractile Fibers". *Journal of Computational Physics,* ***82***(2), June, pp. 289–297.

[8] Basdevant, C., and Sadourny, R., 1984. Numerical Solution of Incompressible Flow: the Mask Method. Laboratoire di Meteorologie Dynamique, Ecole Normale Superieure, Paris.

[9] Briscolini, M., and Santangelo, P., 1989. "Development of the Mask Method for Incompressible Unsteady Flows". *Journal of Computational Physics,* ***84***(1), September, pp. 57–75.

[10] Goldstein, D., Handler, R., and Sirovich, L., 1993. "Modeling No-slip Flow Boundary with an External Force Field". *Journal of Computational Physics,* ***105***(2), April, pp. 354–366.

[11] Fadlun, E. A., Verzicco, R., Orlandi, P., and Mohd-Yosuf, J., 2000. "Combined Immersed-Boundary Finite-Difference Methods for Three-Dimensional Complex Flow Simulations". *Journal of Computational Physics,* ***161***(1), June, pp. 35–60.

[12] Balaras, E., 2004. "Modeling Complex Boundaries Using an External Force Field on Fixed Cartesian Grids in Large-Eddy Simulations". *Computers and Fluids,* ***33***, pp. 375–404.

[13] Majumdar, S., Iaccarino, G., and Durbin, P., 2001. RANS Solvers with Adaptive Structured Boundary Non-Conforming Grid. Annual research briefs, Center for Turbulence Research, Stanford University.

[14] Tseng, Y., and Ferziger, J., 2003. "A Ghost-Cell Immersed Boundary Method for Flow in Complex Geometry.". *Journal of Computational Physics,* ***192***(2), December, pp. 593–623.

[15] Iaccarino, G., 2004. "Immersed Boundary Technique for Turbulent Flows With Industrial Applications". PhD Thesis, Politecnico di Bari.

[16] Dadone, A., and Grossman, B., 2004. Efficient Fluid Dynamic Design Optimization Using Cartesian Grids. Tech. rep., National Aeronautics and Space Administration. Report NASA/CR-2004-213036, NIA-2004-07.

[17] Dadone, A., and Grossman, B., 2007. "Ghost-Cell Method For Inviscid Three-Dimensional Flows on Cartesian Grids". *Computers and Fluids,* ***36***(10), December, pp. 1513–1528.

[18] Poncet, P., 2009. "Analysis of an Immersed Boundary Method for Three-Dimensional Flows in Vorticity Formulation". *Journal of Computational Physics,* ***228***(19), October, pp. 7268–7288.

[19] Borazjania, I., Geb, L., and Sotiropoulosa, F., 2008. "Curvilinear Immersed Boundary Method for Simulating Fluid Structure Interaction with Complex 3D Rigid Bodies". *Journal of Computational Physics,* ***227***(16), August, pp. 7587–7620.

[20] Mulas, M., Chibbaro, S., Delussu, G., Piazza, I. D., and Talice, M., 2002. "Efficient Parallel Computations of Flows of Arbitrary Fluids for all Regimes of Reynolds, Mach and Grashof numbers". *International Journal of Numerical Methods for Heat and Fluid Flow,* ***12***(6), pp. 637–657.

[21] Spalart, P. R., and Allmaras, S. R., 1992. "A One-Equation Turbulence Model for Aerodynamic Flows". *AIAA paper 92-0439*, January. AIAA 30th Aerospace Sciences Meeting and Exhibit, Reno, NV.

[22] Dadone, A., and Grossman, B., 2005. Ghost-Cell Method For Inviscid Three-Dimensional Flows on Cartesian Grids. 43rd AIAA Aerospace Sciences Meeting and Exhibit, Reno, Nevada, 10–13 January.

[23] R., C., K., F., and H., L., 1928. ber die partiellen differenzengleichungen der mathematischen physik. Mathematische Annalen 100 (1), May. Bibcode 1928MatAn.100...32C, doi:10.1007/BF01448839, JFM 54.0486.01, MR 1512478.

[24] Richard W., M., 1996. *Flow measurement engineering handbook*. McGraw-Hill.